REPORT DOCUMENTATION PAGE

Form Approved OMB No. 0704-0188

1. REPORT DATE *(DD-MM-YYYY)*	2. REPORT TYPE	3. DATES COVERED *(From – To)*
16-08-2004	Final Report	1 November 2003 - 01-Aug-04

4. TITLE AND SUBTITLE

Influence Of Niobium On The Dynamic Recrystallization Of Nickel

5a. CONTRACT NUMBER
FA8655-03-M4061

5b. GRANT NUMBER

5c. PROGRAM ELEMENT NUMBER

6. AUTHOR(S)

Dr. Frank J Montheillet

5d. PROJECT NUMBER

5d. TASK NUMBER

5e. WORK UNIT NUMBER

7. PERFORMING ORGANIZATION NAME(S) AND ADDRESS(ES)
Ecole des Mines de Saint-Etienne (ENSM-SE)
158, cours Fauriel
Saint-Etienne Cedex 2 42023
France

8. PERFORMING ORGANIZATION REPORT NUMBER

N/A

9. SPONSORING/MONITORING AGENCY NAME(S) AND ADDRESS(ES)

EOARD
PSC 802 BOX 14
FPO 09499-0014

10. SPONSOR/MONITOR'S ACRONYM(S)

11. SPONSOR/MONITOR'S REPORT NUMBER(S)
SPC 03-4061

12. DISTRIBUTION/AVAILABILITY STATEMENT

Approved for public release; distribution is unlimited.

13. SUPPLEMENTARY NOTES

14. ABSTRACT

This report results from a contract tasking Ecole des Mines de Saint-Etienne (ENSM-SE) as follows: The project will study the influence of niobium in solid solution, without intermetallic precipitates, on dynamic recrystallization of high purity nickel. Nb plays an important role, although not well understood, on the hot deformation mechanisms of superalloys like Inconel 718. Alloys of 0, 0.1, and 1 weight percent niobium will be prepared and studied to determine their dynamic and post-dynamic recrystallization mechanisms and kinetics.

15. SUBJECT TERMS
EOARD, Process Optimization, Metals & alloys, Nickel, Superalloy

16. SECURITY CLASSIFICATION OF:			17. LIMITATION OF ABSTRACT	18, NUMBER OF PAGES	19a. NAME OF RESPONSIBLE PERSON
a. REPORT	b. ABSTRACT	c. THIS PAGE			KEVIN J LAROCHELLE, Maj, USAF
UNCLAS	UNCLAS	UNCLAS	UL	28	19b. TELEPHONE NUMBER *(Include area code)* +44 (0)20 7514 3154

Ecole Nationale Supérieure des Mines
SAINT-ETIENNE

CENTRE NATIONAL DE LA RECHERCHE SCIENTIFIQUE

Center for Materials Science and Structures

Plasticity, Damage, and Corrosion of Materials
CNRS Laboratory

INFLUENCE OF NIOBIUM ON THE DYNAMIC RECRYSTALLIZATION OF NICKEL

EOARD Contract No. FA8655-03-M-4061

Final Report

F. Montheillet, S. Girard-Insardi,
Ch. Desrayaud, and J. Le Coze

July 2004

CONTENTS

I. INTRODUCTION

Dynamic recrystallization (DRX) plays a central role in the hot working processes of metals, since it controls to a large extent the grain sizes and orientations, and therefore the mechanical properties of the final product. DRX mechanisms have been much less investigated in nickel base superalloys than, for instance in steels. This is partly because such alloys contain a large number of addition elements which may interact in a complicated way during hot deformation.

The long term overall objective of our research program is to investigate the influence of interstitial (C) and substitutional (like Cr, Nb, Mo) solutes, as well as precipitates (like Ni_3Nb) most commonly present in nickel base structural alloys on their dynamic and post-dynamic recrystallization mechanisms and kinetics. Such research aims at providing the necessary basic knowledge, from which optimized hot working schedules can be more rationally and efficiently tailored by production engineers.

The behaviour of Nb in nickel base alloys is particularly questionable: it is well known that segregations resulting from solidification with a spatial scale corresponding to that of the dendritic microstructure (≈ 200 to 400 µm) are not wiped out by hot working. For instance, in an Inconel 718 grade containing 5 wt%Nb, concentration fluctuations of about ± 0.2 %Nb have been measured (Thomas, 2004). This indicates that the bulk diffusion of niobium is slow, even during high temperature deformation. On the other hand, estimated grain boundary mobilities in two Inconel grades containing 5.0 and 5.4 wt%Nb, respectively, were significantly different, which shows that Nb solutes interact with grain boundaries. This suggests in turn that Nb solutes are able to migrate with grain boundaries. Other observations seem to show that they are able to move with dislocations as well.

Within the general frame of the program, the present limited research deals therefore with the influence of niobium in *solid solution* (i.e., without intermetallic precipitates) on DRX of pure nickel. Model materials were used for the hot deformation tests and subsequent microstructural investigations. In this final report, their preparation, transformation and characterization are first described; the investigation of their mechanical behaviour during hot torsion is then reported, and the associated microstructures and textures are analyzed from EBSD observations. Finally, the above set of data is used to discuss the influence of niobium on the hot deformation mechanisms of nickel.

II. PREPARATION AND TRANSFORMATION OF THE MODEL MATERIALS

Three batches were prepared: high purity nickel (referred to as Ni below), and two Ni-Nb alloys containing nominally 0.1 and 1.0 wt%Nb, (Ni-0.1Nb, and Ni-1Nb, respectively). According to the Ni-Nb phase diagram, Nb is entirely in solid solution within the hot working range of both alloys (Figure 1): at 600 °C, the maximum solubility is about 6 at%, which is tantamount to 9 wt% using the atomic weights m_{Nb} = 92.9 g and m_{Ni} = 58.71 g.

II.1. High purity nickel (Ni)

It was prepared from commercial electrolytic purity material. The chemical composition, as provided by the supplier, is given in Table 1. In the same table, the main impurity content of a nickel used by Luton and Sellars (1969) is also reported, which shows that purity of the present material is much better.

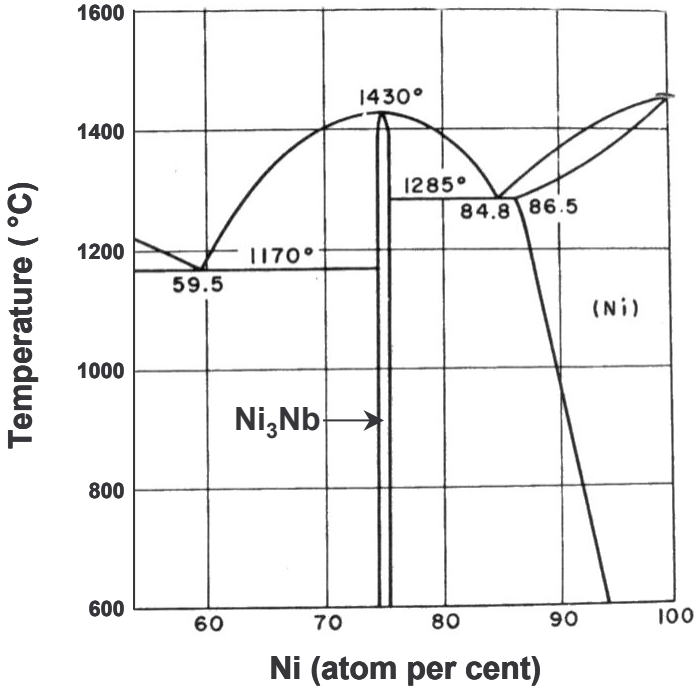

Figure 1. Ni rich part of the Ni-Nb phase diagram.

Table 1. Chemical composition of the nickel (wt. ppm, balance = Ni).

	As	Bi	Co	Cu	Fe	Mn	Pb	Sb	Si	Zn	C	S	O	N
As received (max. value)	0.5	0.2	0.5	10	150	-	0.5	0.5	5	0.5	150	15	-	-
Luton and Sellars (1969)	-	-	-	100	500	100	-	-	100	-	40	-	-	-
After purification	-	-	-	-	150	-	-	-	-	-	≈ 5	≤ 5	≈ 6	≤ 5

This material was then purified by induction melting in a cold silver crucible under high purity argon-hydrogen atmosphere, using a procedure developed for a long time in the laboratory (Le Coze et al., 1995), as illustrated in Figure 2. The induction coil is displaced several (*e.g.*, 9) times from the left to the right of the crucible and back. The whole process is repeated 7 times with intermediate cleaning of the device. The Fe content is not modified by purification, but the contents in C, S, N, and O are reduced to about 5 ppm or less, as shown in Table 1 (Leco method).

It should be noted that ultra-high purity nickel could be prepared as well, however it is ten times more expensive than the above high purity grade, which can be considered as relevant for the first step of the present investigation.

Figure 2. Induction melting device used for purification of the model materials.

II.2. Nickel-niobium alloys (Ni-0.1Nb and Ni-1Nb)

Commercial purity niobium (99.9 %) was added to the melt for preparing the two Ni-Nb alloys using the same cold crucible as above. The niobium, oxygen, and carbon contents were measured by various methods, as shown in Table 2.

Table 2. Nb, O, and C contents of the two Ni-Nb alloys
([1]Inductive Coupling Plasma; [2]Atomic Absorption; [3]Spark Emission Spectroscopy).

	Nb (%)				O (ppm)	C (ppm)
Alloy	ICP[1]	AA[2]	SES[3] 1	SES[3] 2	Leco	
Ni-0.1Nb	0.092	-	-	a-0.070 b-0.082 c-0.091	6.8	3.9
Ni-1Nb	0.953	0.79	a-0.66 b-0.76 c-0.79	a-0.742 b-0.797 c-0.826	4.5	6.2

It appears that for some reason, a fraction of Nb was lost during preparation, which does not seem to occur for Fe-Nb alloys. Spectrometry measurements were carried

out on three points of the ingot, a and c are associated with the first and last parts to be solidified during the last displacement of the induction coil, respectively, whereas b corresponds to the half length of the ingot. Results reported in Table 2 seem to suggest that some macro-segregation occurs, although this should be confirmed. Oxygen and carbon contents are quite similar to values measured in purified nickel.

II.3. Transformation

From each of the three ingots (Ni, Ni-0.1Nb, and Ni-1Nb) of weight about 1.2 kg, 200 g were removed for the above chemical analyses. The remaining part was hot forged using a power hammer at 1050 °C (starting temperature) into cylindrical bars of diameter 14 mm (Figure 3). The latter were then reduced at 1050 °C to a diameter of 10 mm by hot swaging.

Figure 3. Power hammer used for the forging of the model alloys.

III. INITIAL MICROSTRUCTURES

A microstructural investigation was carried out by optical microscopy on the three materials in the wrought state (i.e., after hot swaging), and after a homogenization heat treatment of 1 h at 700 °C. Such intermediate temperature was chosen for avoiding grain growth. Figures 4a, c, and e show that the initial grain size of Ni and Ni-0.1 Nb is close to 500 µm, while it is much smaller (50-100 µm) in Ni-1Nb. They are not significantly changed by the heat treatment, as shown by Figures 4b, d, and f. For further hot deformation experiments, it could be relevant to homogenize the Ni-1Nb grade at higher temperature to get an initial grain size closer to that of the other two materials.

Microhardness measurements were also carried out on the three grades in the wrought and heat-treated states, as reported in Table 3. Some softening after heat-treatment is observed for Ni and Ni-0.1Nb, whereas such effect is negligible for Ni-1Nb. This can be associated with dislocation recovery, that would be hindered by Nb solutes in the last alloy.

Table 3. Microhardness of the three grades in the wrought state and after heat-treatment (Hv, load: 100 g, average of 10 measurements)

	Wrought	Heat-treated
Ni	147	112
Ni-0.1Nb	123	109
Ni-1Nb	151	148

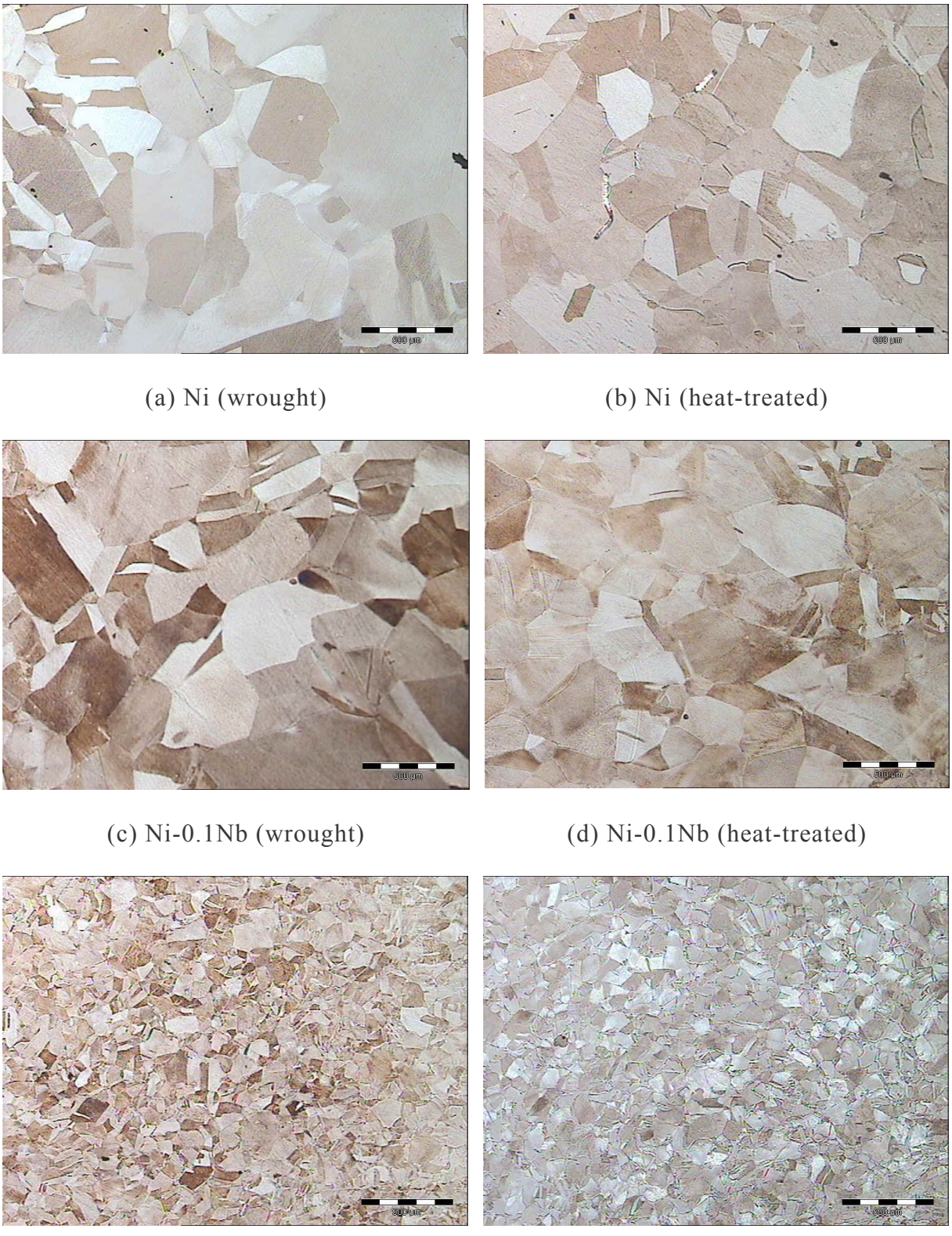

(a) Ni (wrought) (b) Ni (heat-treated)

(c) Ni-0.1Nb (wrought) (d) Ni-0.1Nb (heat-treated)

(e) Ni-1Nb (wrought) (f) Ni-1Nb (heat-treated)

Figure 4. Initial microstructures of the model materials in the wrought state and after heat treatment for 1 h at 700 °C
(optical metallography; half-length of the bar; scale length: 500 µm).

IV. MECHANICAL BEHAVIOUR DURING HOT WORKING

IV.1. Hot torsion testing procedure

Torsion was used in the present study, since it is more suited than compression or tension tests to achieve large strains under well-controlled strain gradient conditions, as well as the associated steady state deformation ranges. About 10 hot torsion specimens (6 mm diameter and 27 mm gauge length) were machined from each of the bars, according to the drawing of Figure 5. Torsion tests were carried out on an electromechanical computer controlled machine. Specimens were all quenched immediately after straining, using a room temperature flow of helium automatically triggered by the processor. This leads to a cooling rate of about 100 °C/s at the beginning of cooling.

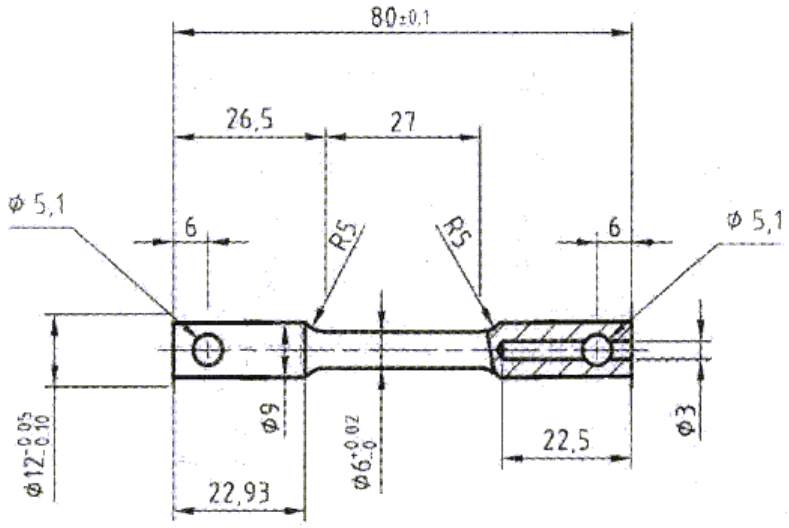

Figure 5. Drawing of the hot torsion specimen

Table 4 displays the applied temperatures and strain rates.

Table 4. Temperature and strain rate conditions of the torsion tests carried out on the three alloys.

	θ (°C)					
$\dot{\bar{\varepsilon}}$ (s^{-1})		800	850	900	950	1000
	0.03	○ ◎ ●		○ ◎ ●		◎ ●
	0.10	○ ◎ ●	○◎●	○ ◎ ●	○◎●	○ ◎ ●
	0.30	○ ◎ ●		○ ◎ ●		○ ◎ ●

○ Pure Ni ◎ Ni-0.1Nb ● Ni-1Nb

Considering the limited number of available specimens when model materials are concerned, it was initially planned to work at a given strain rate in this first step, and to use literature data for the strain rate sensitivities that are required for flow stress determinations. A first series of torsion tests was thus carried out at $\dot{\bar{\varepsilon}} = 0.1\,s^{-1}$ and five temperatures from 800 to 1000 °C. According to Luton and Sellars (1969), the "engineering" strain rate sensitivity $\tilde{m} = \partial \ln \Gamma / \partial \ln \dot{N}$, where Γ is the torsion torque and $\dot{N}$ the speed of revolution, was taken equal to 0.18 for pure nickel (average value within the temperature range), and supposed to remain unchanged for the two Ni-Nb alloys[1].

Although such estimation of $\tilde{m}$ is questionable since the above authors used much less pure nickel (see Table 1), and the influence of niobium on strain rate sensitivity is not known, the approximation is justified from consideration of the Fields and Backofen equation:

$$\sigma = \frac{\sqrt{3}\,\Gamma}{2\pi R_0^3}\left(3 + \tilde{m} + \tilde{n}\right) \qquad (1)$$

where R_0 is the outer specimen radius, and $\tilde{m}$ and $\tilde{n}$ the "engineering" rheological parameters $\tilde{m} = \partial \ln \Gamma / \partial \ln \dot{N}$ and $\tilde{n} = \partial \ln \Gamma / \partial \ln N$. It shows that the influence of the strain rate sensitivity parameter $\tilde{m}$ on the flow stress σ is quite low. More precisely:

$$\frac{\Delta\sigma}{\sigma} = \frac{\Delta\Gamma}{\Gamma} + \frac{\Delta\tilde{m} + \Delta\tilde{n}}{3 + \tilde{m} + \tilde{n}} \qquad (2)$$

Thus for an absolute error on $\tilde{m}$ as large as $\Delta\tilde{m} = 0.1$, the resulting relative error on the flow stress would be less than $\Delta\tilde{m}/3 \approx 3.3\,\%$.

By contrast, the above approach is no longer valid for determination of the apparent activation energy Q associated with hot deformation. The latter is generally derived from $\ln\sigma - 1/T$ plots, where the slope of the curve is mQ/R (T is the absolute deformation temperature, R the gas constant). Obviously, even a small error on m involves a large variation of Q derived from the measured product mQ.

Therefore, additional tests were performed on a few spared specimens to determine the strain rate sensitivities of the three materials at 800, 900, and 1000 °C, as shown in Table 4 (for Ni at 1000 °C, only one extra test was carried out at 0.3 s^{-1}).

IV.2. Stress-strain curves

Figures 6a-c display stress-strain curves of the three materials at $\dot{\bar{\varepsilon}} = 0.1\,s^{-1}$ within the temperature range 800-1000 °C (≈ 0.62-0.74 T_m). There is no evidence of significant self-heating at this strain rate. Not only the stress level, but also the shape

[1] It should be noted that whenever the "engineering" strain rate sensitivity $\tilde{m}$ is independent of strain rate, it identifies with the strain rate sensitivity m of the flow stress.

of the flow curves, is strongly modified by the addition of niobium. For pure nickel, steady state flow stress is attained at strains ε_S from about 0.5 at 1000 °C to 1.0 at 800 °C, whereas ε_S falls between the ranges 1 to 3 for Ni-0.1 Nb, and 2 to 3.5 for Ni-1Nb.

The slight irregular oscillations occurring on some of the curves pertaining to Ni and Ni-0.1Nb are not thought to reflect some specific dynamic recrystallization mechanism, but rather experimental artifacts linked for instance to the large initial grain sizes. Indeed, no oscillations are observed for Ni-1Nb with displays a smaller grain size (see first report). All the flow curves therefore belong to the single peak type classically associated with discontinuous dynamic recrystallization. For pure nickel, this is in agreement with the results of Luton and Sellars (1969): these authors observed multiple peak flow curves only when the large strain flow stress level was less than about 41 MPa, which corresponds to the minimum steady state flow stress reached in the present investigation (at 1000 °C). For the Ni-Nb alloys it is not surprising that multiple peak flow curves are not observed, since niobium in solid solution is expected to decrease grain boundary mobility, and thus to limit grain growth normally associated with wavy flow curves.

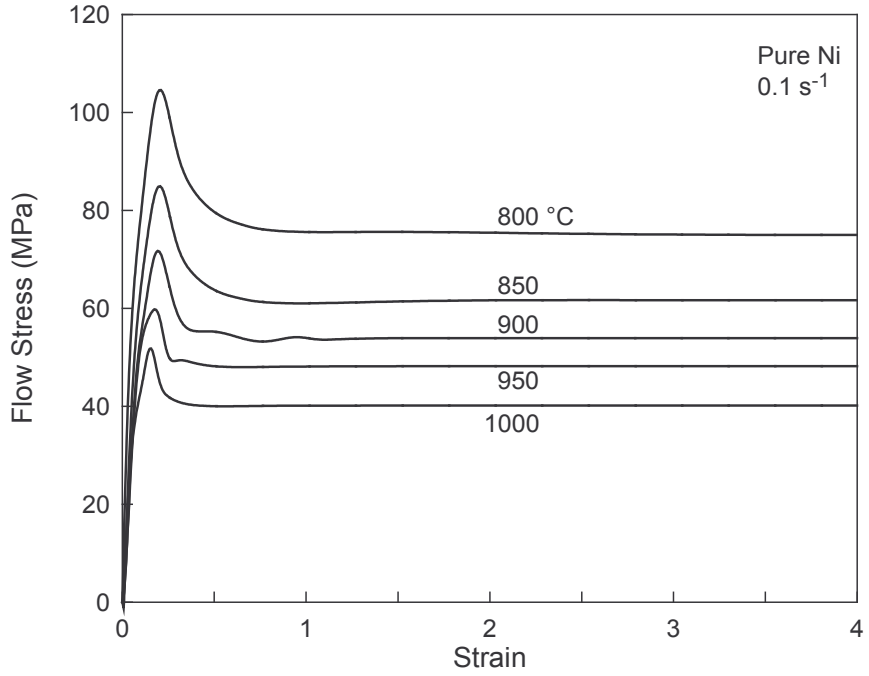

Figure 6a. Stress-strain curves obtained from hot torsion tests on the pure nickel at $\dot{\bar{\varepsilon}} = 0.1\,s^{-1}$

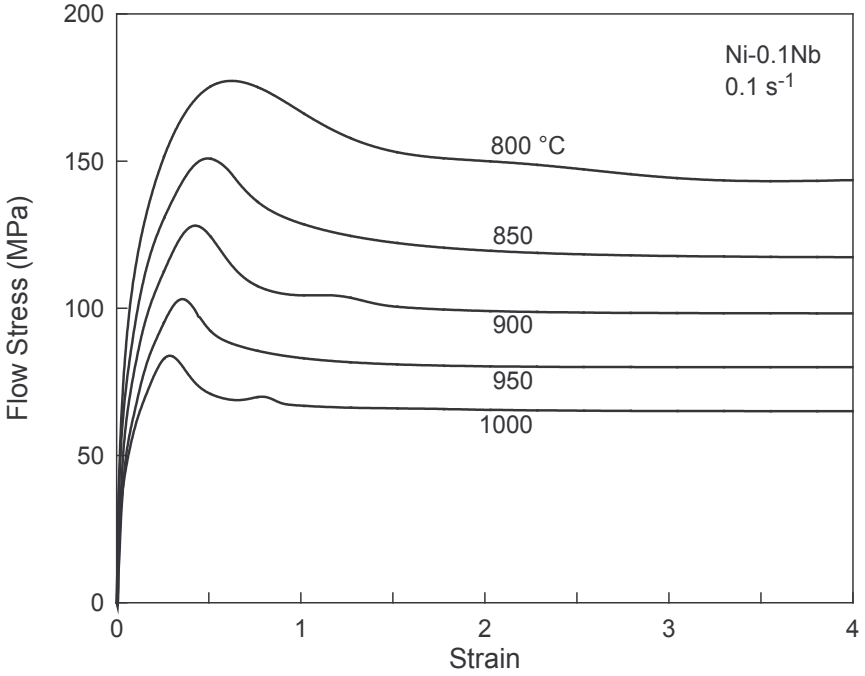

Figure 6b. Stress-strain curves obtained from hot torsion tests on the high purity base Ni-0.1Nb alloy at $\dot{\varepsilon} = 0.1\,s^{-1}$

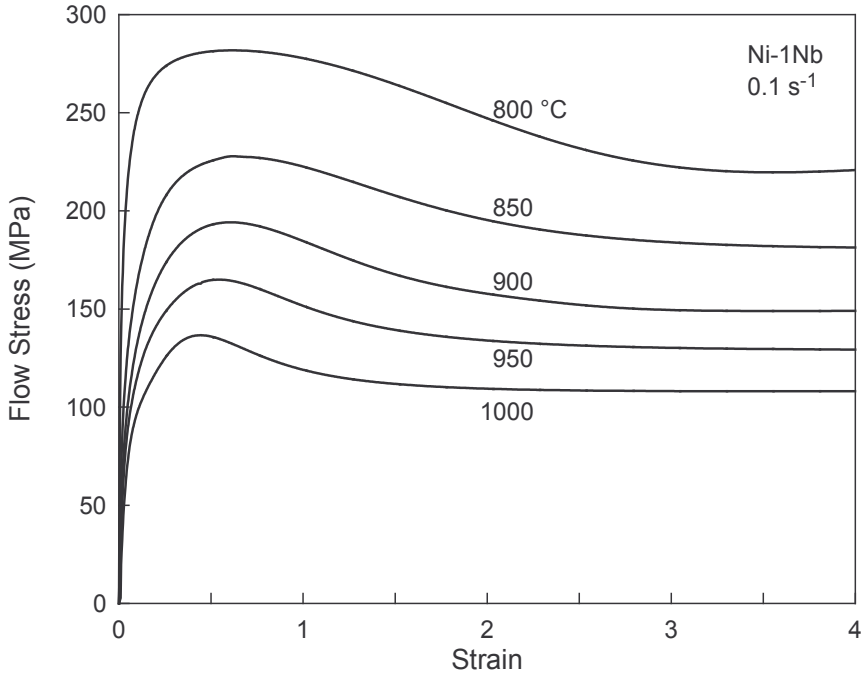

Figure 6c. Stress-strain curves obtained from torsion tests on the high purity base Ni-1Nb alloy at $\dot{\varepsilon} = 0.1\,s^{-1}$

IV.3. Strain rate sensitivity

"Engineering" strain rate sensitivities $\tilde{m}$ derived from $\log\Gamma - \log\dot{\bar{\varepsilon}}$ plots[2] are reported in Table 5 for the three materials at 800, 900, and 1000 °C. In each case, two values of $\tilde{m}$ were determined, corresponding to the maximum torque and the steady state torque ($\bar{\varepsilon}$ = 5), respectively. Since the points were perfectly aligned in the various $\log\Gamma - \log\dot{\bar{\varepsilon}}$ diagrams, $\tilde{m}$ is independent of strain rate within the investigated range. Furthermore, in the two above conditions $\tilde{n} = 0$, therefore $m = \tilde{m}$ according to eq.(1).

Table 5. Strain rate sensitivities m_M (maximum torque) and m_S (steady state torque) of the three materials.

	m_M			m_S		
Temp. (°C)	Ni	Ni-0.1Nb	Ni-1Nb	Ni	Ni-0.1Nb	Ni-1Nb
800	0.203	0.096	0.110	*0.131*	0.081	*0.156*
900	0.198	0.140	0.113	0.153	0.110	0.100
1000	*0.143*	0.167	0.142	0.149	0.137	0.107

Values in italics are considered are less reliable, generally because of self-heating. It can therefore be concluded that:

- the strain rate sensitivities of the three alloys increase slightly with temperature in the range 800–1000 °C;
- they are much smaller for Ni-0.1Nb than for pure nickel; however, further addition of niobium up to 1 % leads to limited decrease of m, as illustrated in Figure 7 at 900 °C.

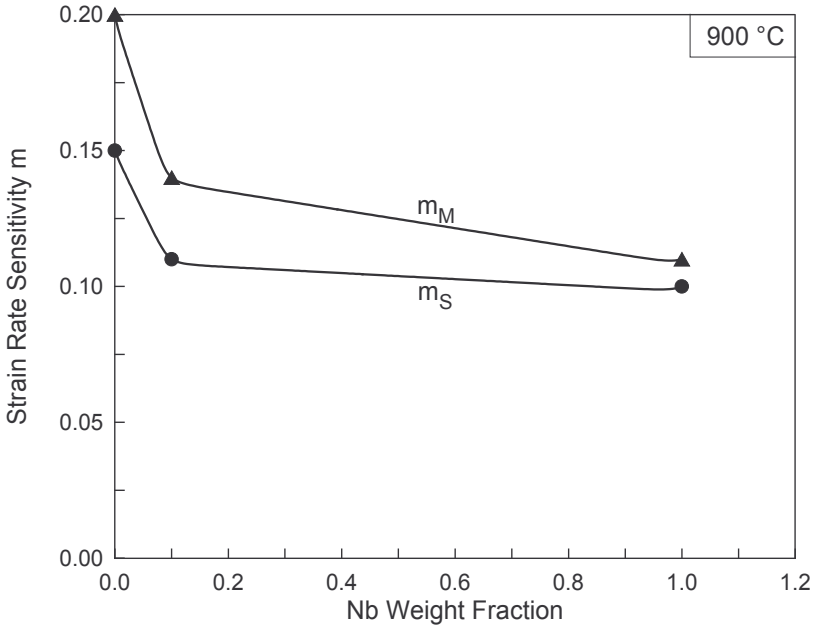

Figure 7. Influence of niobium content on the strain rate sensitivities m_M (maximum torque) and m_S (steady state torque) at 900 °C (values rounded to the second decimal digit)

[2] Note that the slopes of the $\log\Gamma - \log\dot{N}$ and $\log\Gamma - \log\dot{\bar{\varepsilon}}$ curves are the same, since $\dot{N}$ and $\dot{\bar{\varepsilon}}$ are proportional

IV.4. Temperature dependence of the flow stress

As mentioned above, the apparent activation energies of hot deformation were derived at $\dot{\varepsilon} = 0.1\,s^{-1}$ for both the peak and steady state stresses from $\ln\sigma - 1/T$ diagrams (*Neperian* logarithm), where T is the absolute deformation temperature (Figures 8a-c). It is worth to note that data are perfectly fitted by straight lines in all cases. Following the classical analysis of strain rate and temperature dependence of flow stress, this means that mQ/R is independent of temperature, where m is the strain rate sensitivity, Q the apparent activation energy, and R the gas constant. Figure 9 shows the influence of niobium content on the above quantity. For both the peak stress and the steady state stress, mQ/R is first increased by the presence of 0.1 %Nb, but then decreases slowly with further niobium addition.

The activation energies Q_M and Q_S pertaining to the maximum and steady state flow stress, respectively, are plotted in Figure 10 *vs* the niobium content[3]. For pure Ni, $Q_M \approx 200$ kJ/mol is significantly less than the value of 234 kJ/mol found by Luton and Sellars (1969). For the two Ni-Nb alloys, Q_M and Q_S are much larger than the activation energies of pure nickel, but the main increase is produced by the presence of 0.1 %Nb, whereas further addition of niobium up to 1 % has again much less effect on the level of Q.

The influence of niobium on the apparent activation energies can be explained simply by the interaction of Nb solutes with grain boundaries and/or dislocations, which is more efficient at lower temperatures. Flow stress is therefore less increased at high than low temperatures, which leads to an increase in slope of the log $\sigma - 1/T$ curves.

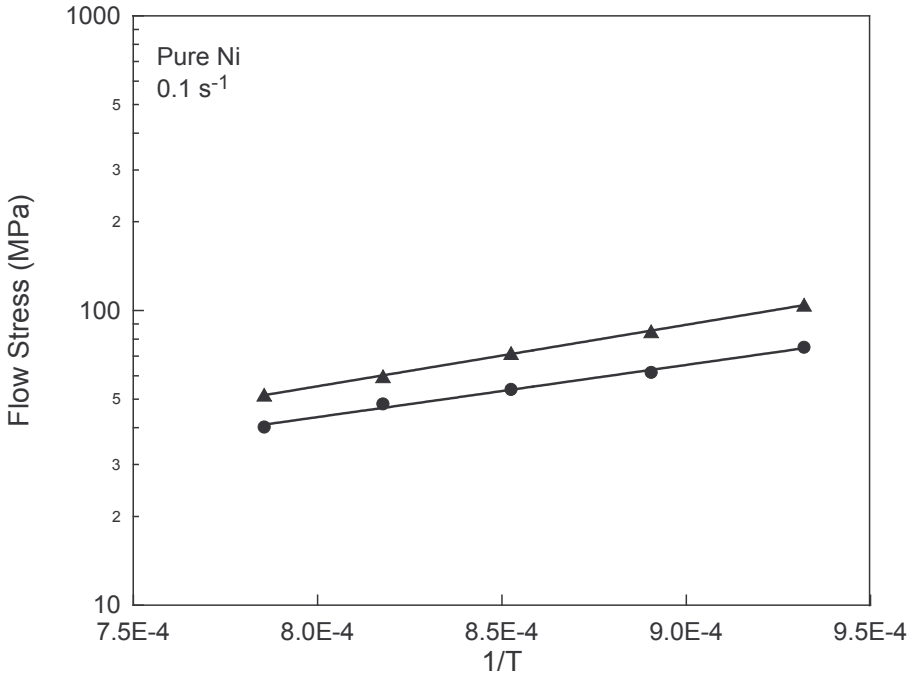

Figure 8a. Peak (▲) and steady state (●) flow stresses plotted *vs.* the inverse absolute temperature for the pure nickel at $\dot{\varepsilon} = 0.1\,s^{-1}$

[3] Note that these results differ slightly from that given in the Second Interim Report, due to the improved evaluation of the strain rate sensitivity parameters m

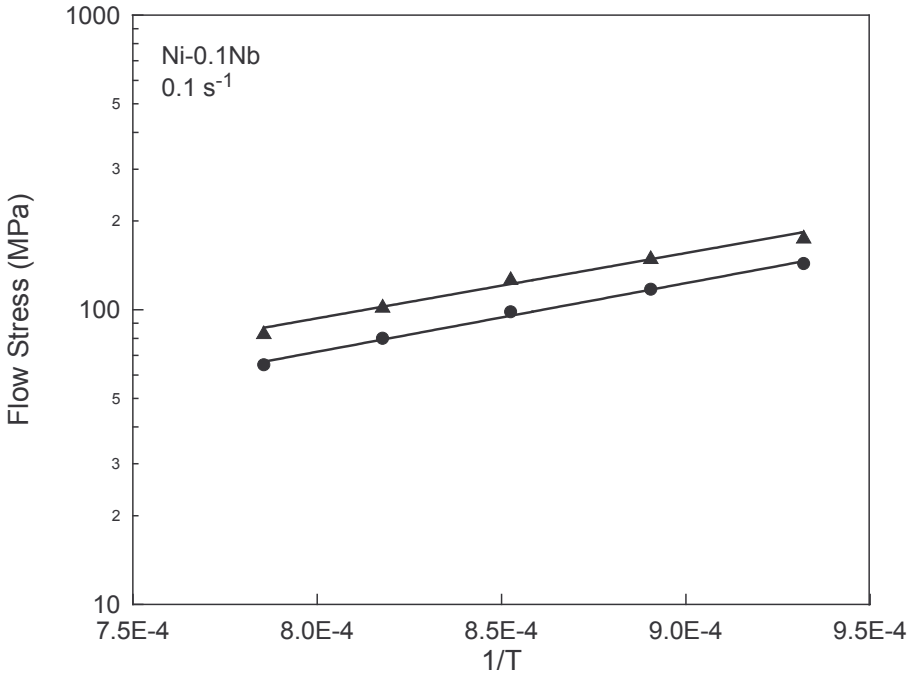

Figure 8b. Peak (▲) and steady state (●) flow stresses plotted *vs.* the inverse absolute temperature for the high purity base Ni-0.1Nb alloy at $\dot{\varepsilon} = 0.1\,s^{-1}$

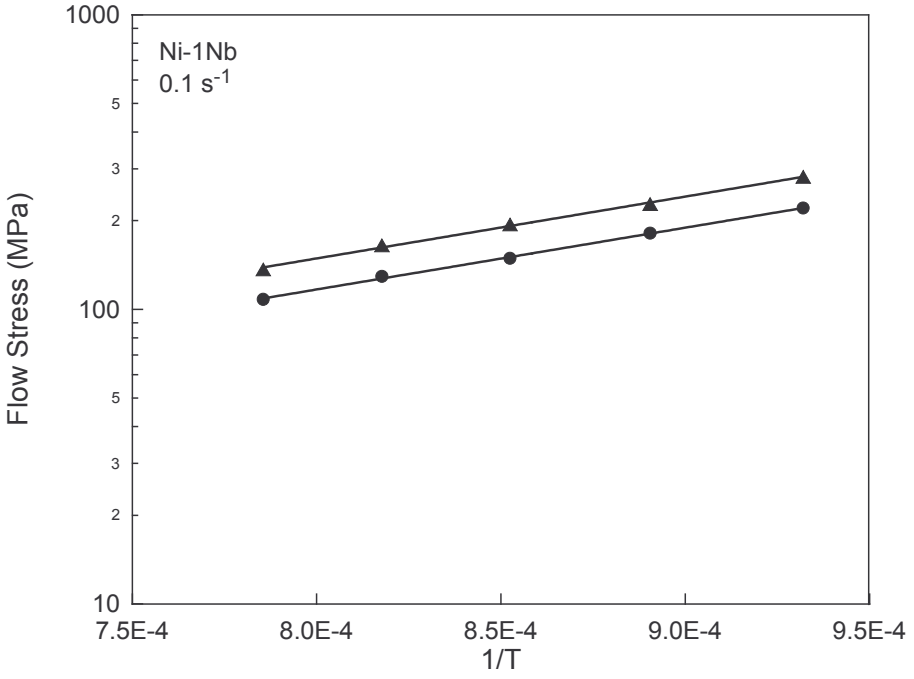

Figure 8c. Peak (▲) and steady state (●) flow stresses plotted *vs.* the inverse absolute temperature for the high purity base Ni-1Nb alloy at $\dot{\varepsilon} = 0.1\,s^{-1}$

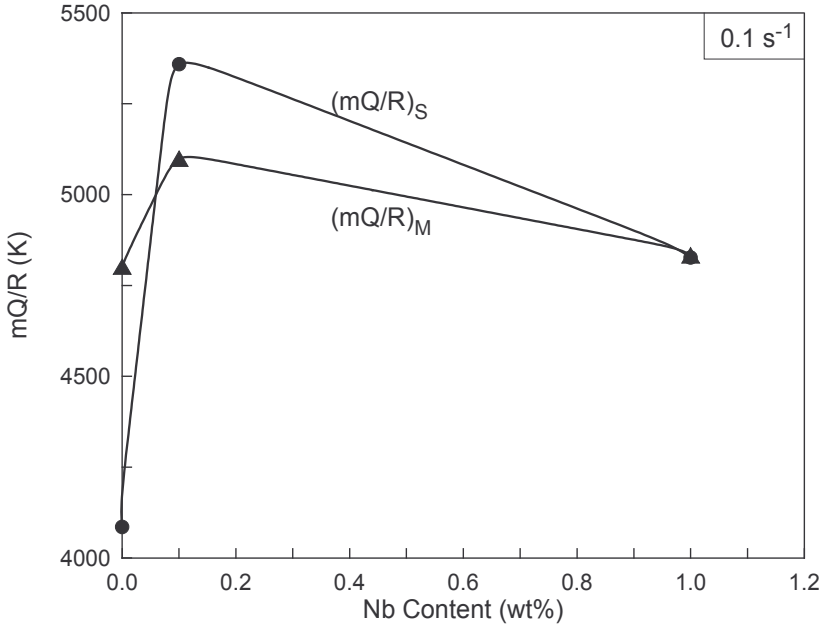

Figure 9. Influence of Nb content on the slope mQ/R of the ln σ-1/T plots for the maximum and steady state flow stress

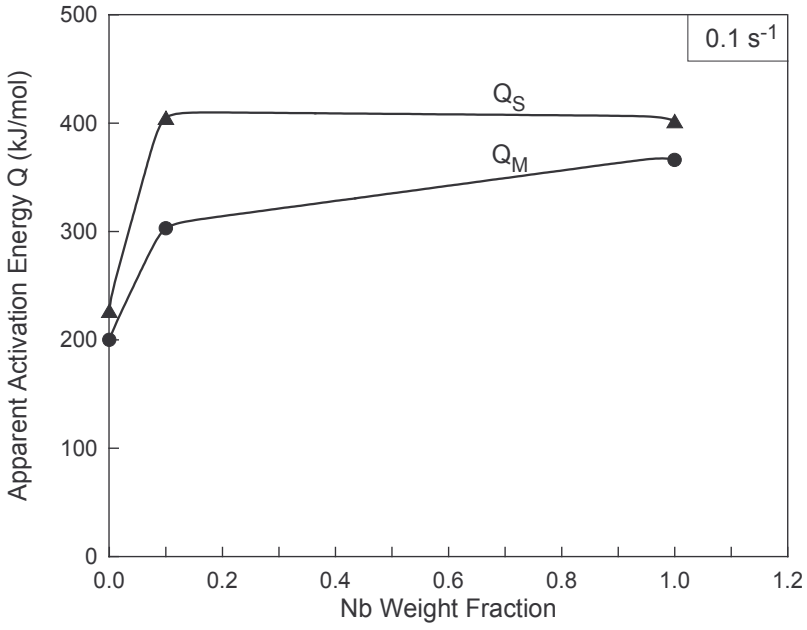

Figure 10. Influence of niobium content on the apparent activation energies Q_M and Q_S at 0.1 s^{-1} determined from the peak stress and steady state stress, respectively

IV.5. Hardening effect of niobium

The influence of niobium content on the maximum and steady state flow stress levels is illustrated in Figures 11a-b for the five temperatures investigated at $\dot{\varepsilon} = 0.1\,s^{-1}$. The hardening effect may be tentatively described by the following simple power law equation:

$$\sigma = \sigma_0 + k\,x^p \qquad (3)$$

where x is the niobium content (wt%), σ_0 the flow stress of pure niobium, and $k = \sigma_1 - \sigma_0$, where σ_1 is the flow stress of Ni-1Nb. It is worth to note that, for both the peak and steady state stresses, the values of exponent p are quite similar, with an average of 0.38.

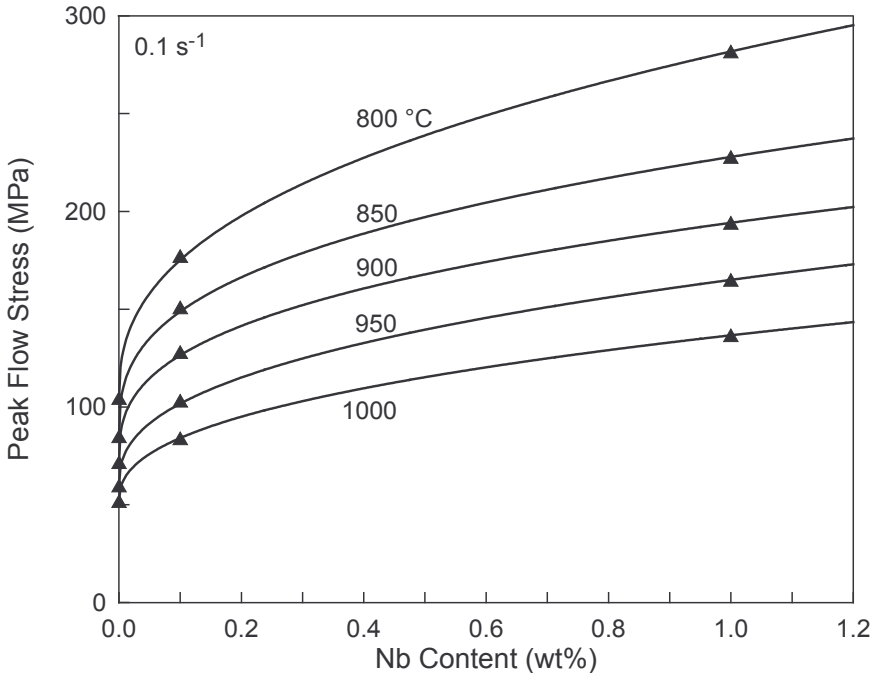

Figure 11a. Influence of niobium content on the maximum flow stress levels at various temperatures

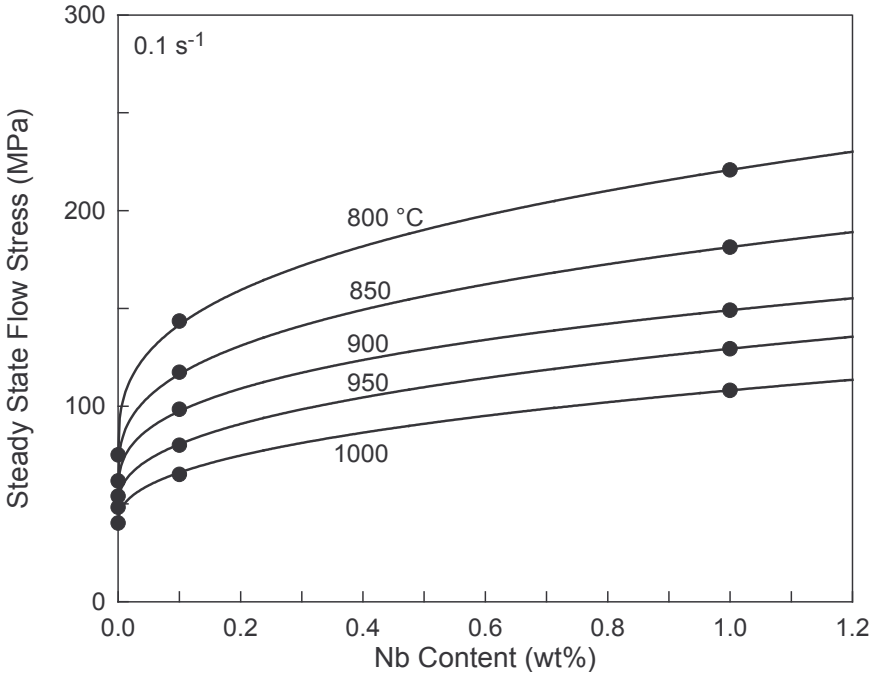

Figure 11b. Influence of niobium content on the steady state flow stress levels at various temperatures

V. HOT DEFORMATION MICROSTRUCTURES

Microstructure and texture investigations were carried out by Electron BackScattering Diffraction (EBSD) on torsion specimens of each of the three materials deformed under the same conditions, *viz.* 900 °C, 0.1 s^{-1}, and a strain of 5, associated with steady state flow stress (but not necessarily steady state microstructure and texture).

In Figures 12a-c, only high angle boundaries (HAB) associated with a misorientation angle larger than 15 deg are represented (including twin boundaries). The microstructure, which appears as well recrystallized, is obviously much finer for Ni-0.1Nb (mean linear intercept: 16.5 µm, Figure 12b) than for pure nickel (152 µm, Figure 12a). In Ni-1Nb, further microstructure refinement leads to an intercept of 5.6 µm (Figure 12c).

In Figures 13a-c, special boundaries are specified by different colours: low angle boundaries (LAB) are identified by a range of gray → pink → red lines corresponding to misorientation angles increasing from 2 deg (detection limit) to 15 deg. Green lines correspond in turn to twin boundaries, *i.e.* boundaries associated with a rotation of 60 deg around a <111> crystallographic axis. A more quantitative description of the fraction areas associated with the various types of boundaries is given by the misorientation angle distributions (Figure 14a-c).

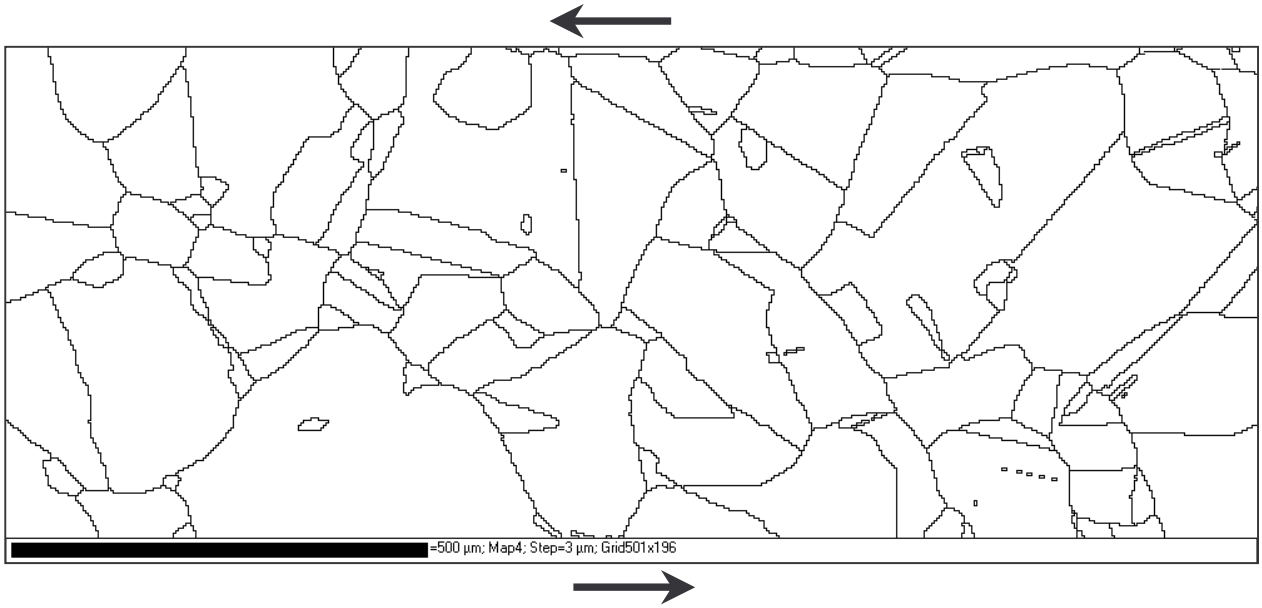
=500 µm; Map4; Step=3 µm; Grid501x196

(a)

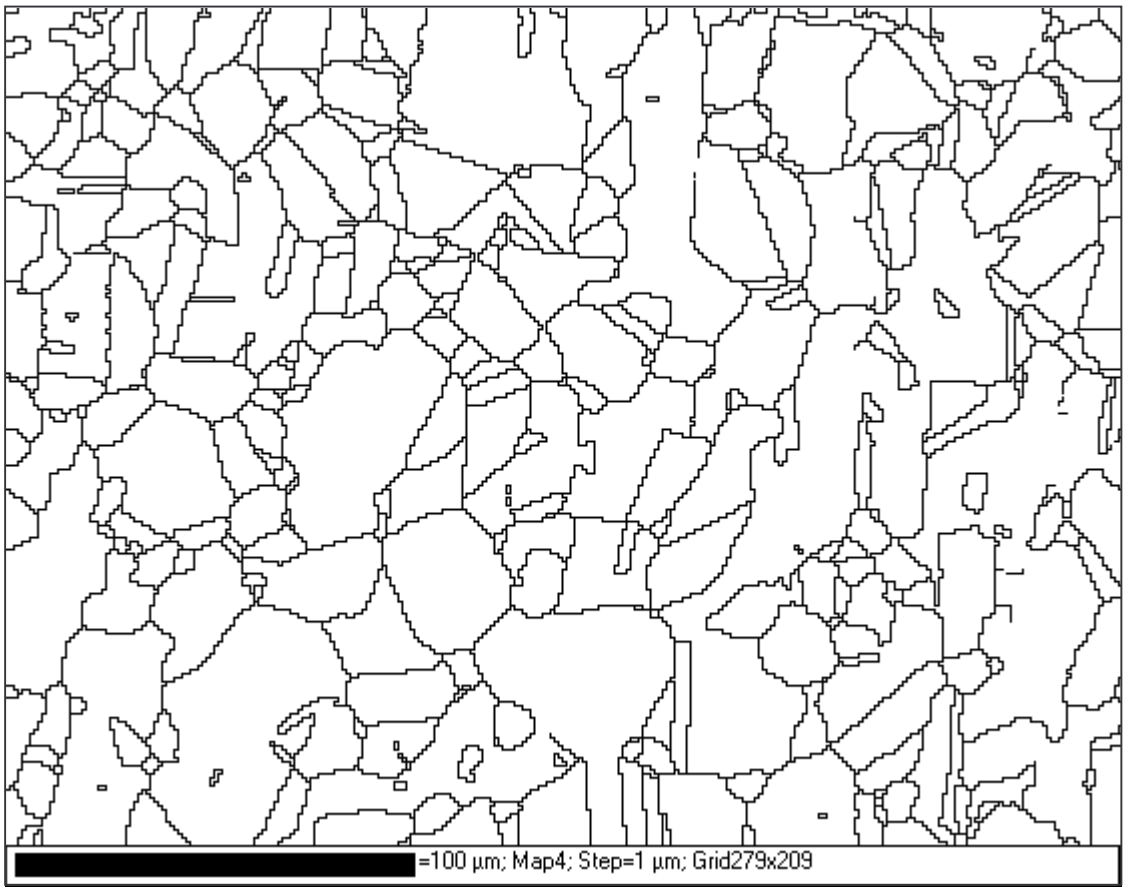
=100 µm; Map4; Step=1 µm; Grid279x209

(b)

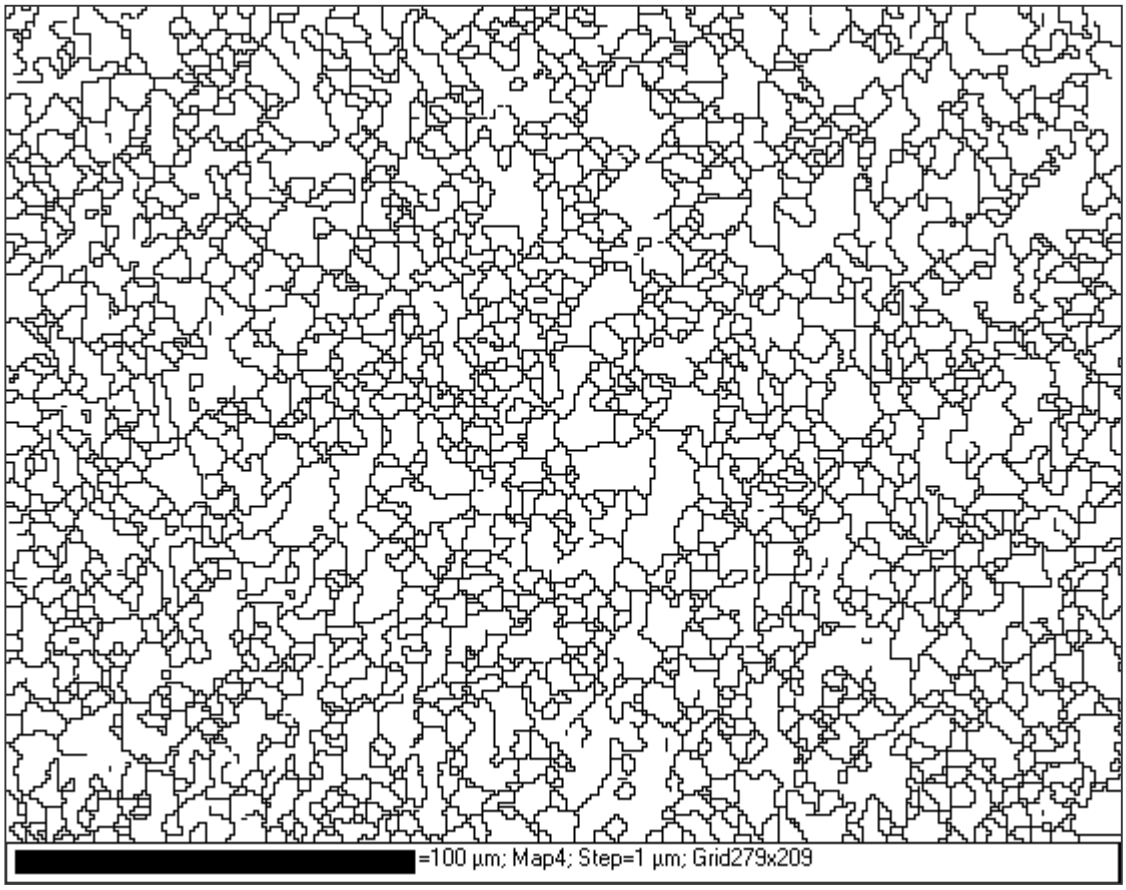

(c)

Figure 12. EBSD maps of the high angle boundaries in pure nickel (a), Ni-0.1Nb (b), and Ni-1Nb (c) after torsion at 900 °C and 0.1 s^{-1} to a strain of 5. Arrows indicate the shear direction.

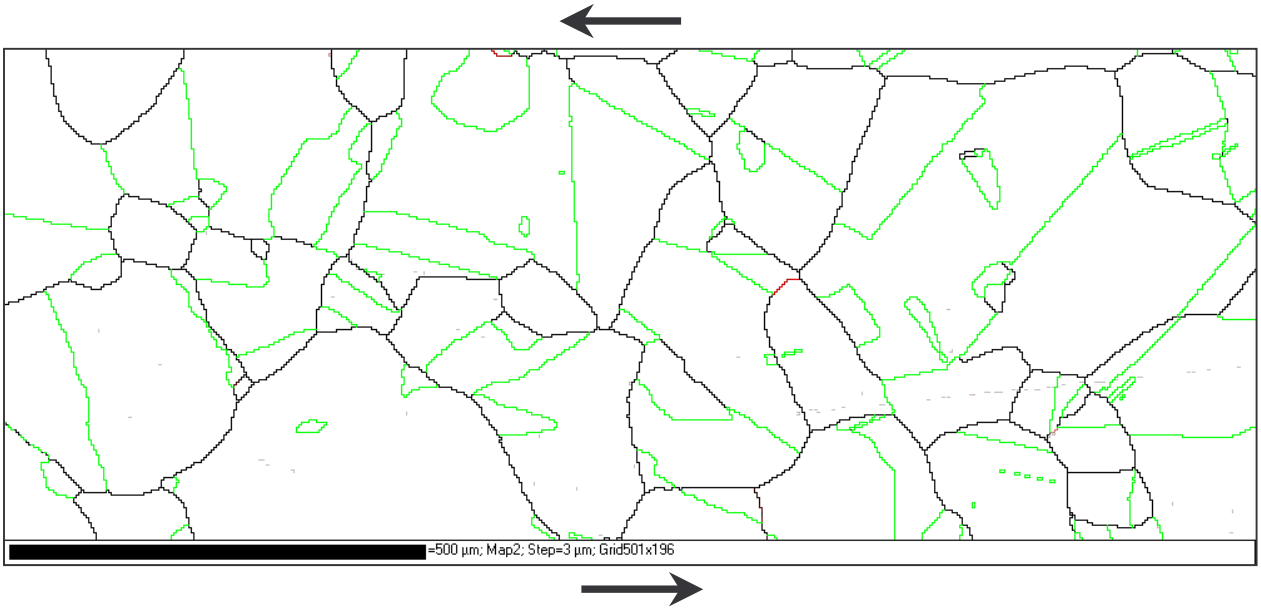
=500 µm; Map2; Step=3 µm; Grid501x196

(a)

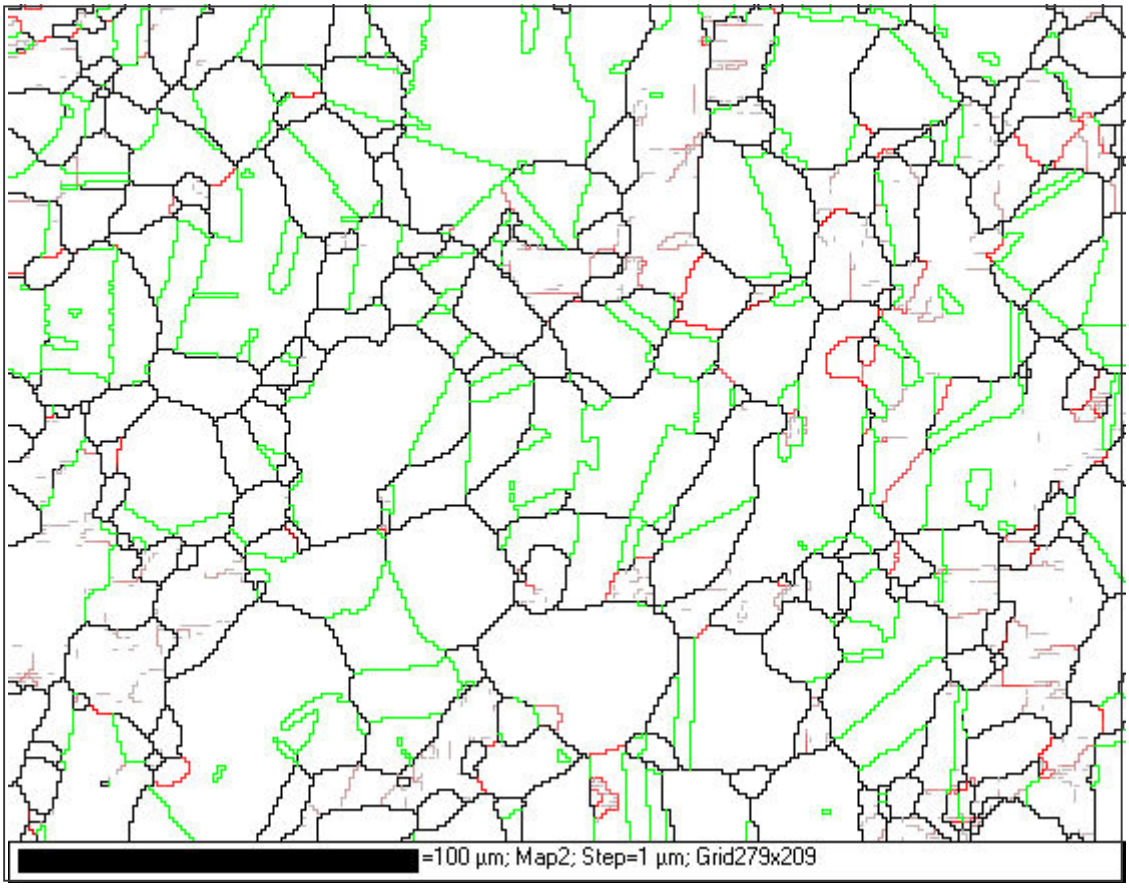
=100 µm; Map2; Step=1 µm; Grid279x209

(b)

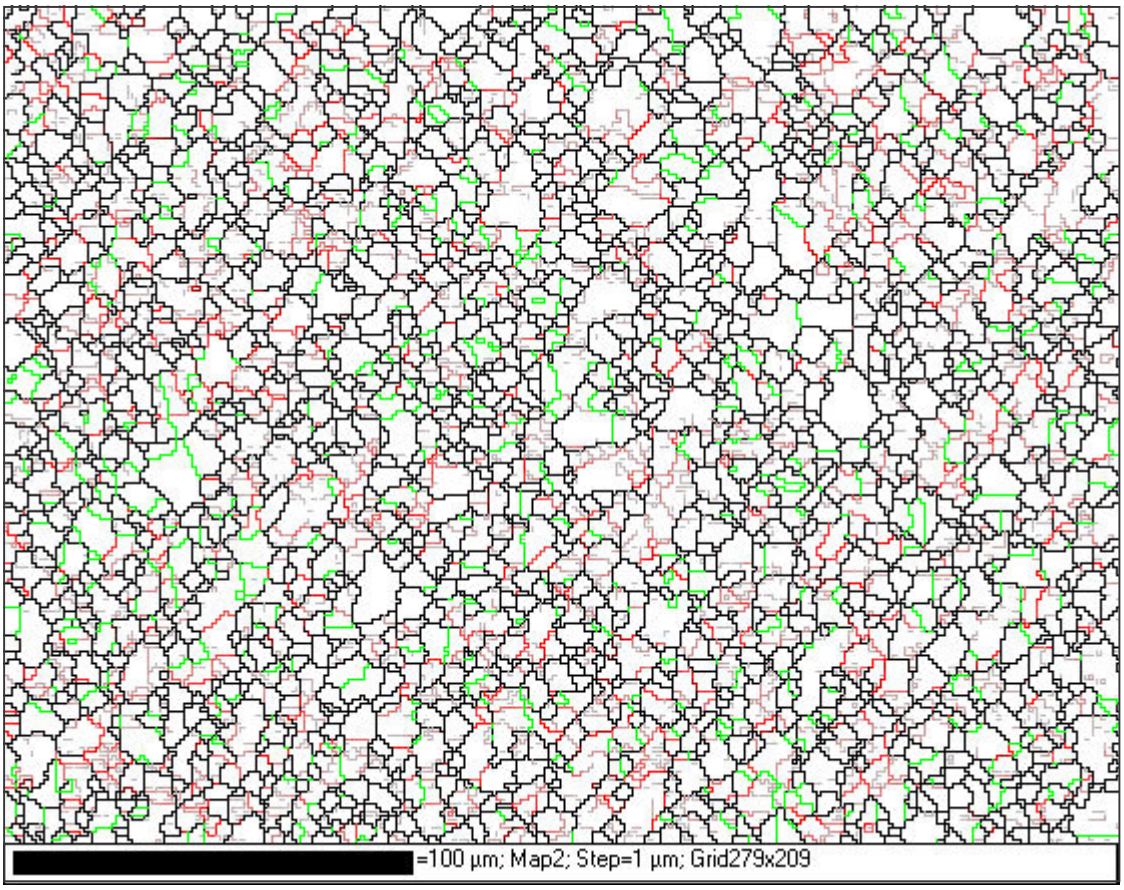

(c)

Figure 13. EBSD maps depicting the various types of boundaries in pure nickel (a), Ni-0.1Nb (b), and Ni-1Nb (c) after torsion at 900 °C and 0.1 s^{-1} to a strain of 5. Arrows indicate the shear direction
(black: ordinary HAB; green: twin boundary; grey-pink-red: LAB)

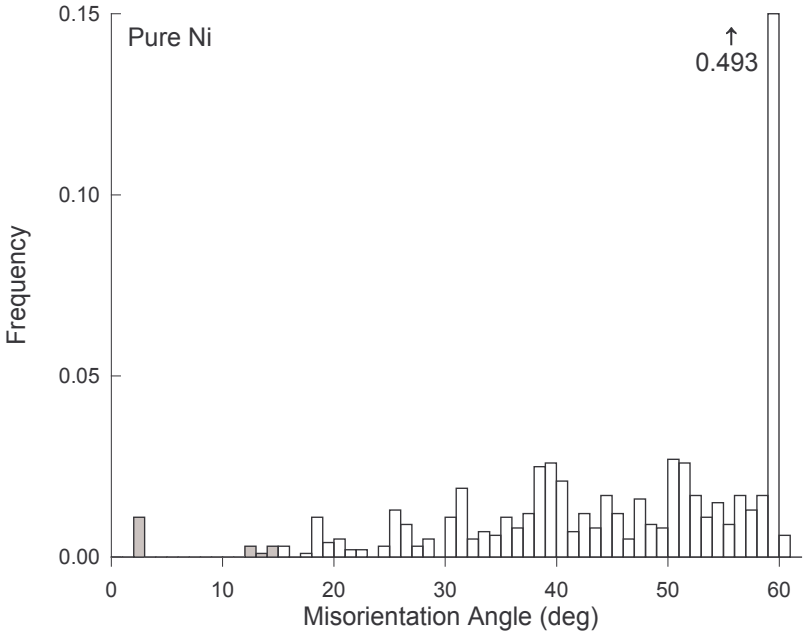
Pure Ni
↑
0.493
Frequency
0.15
0.10
0.05
0.00
0
10
20
30
40
50
60
Misorientation Angle (deg)

(a)

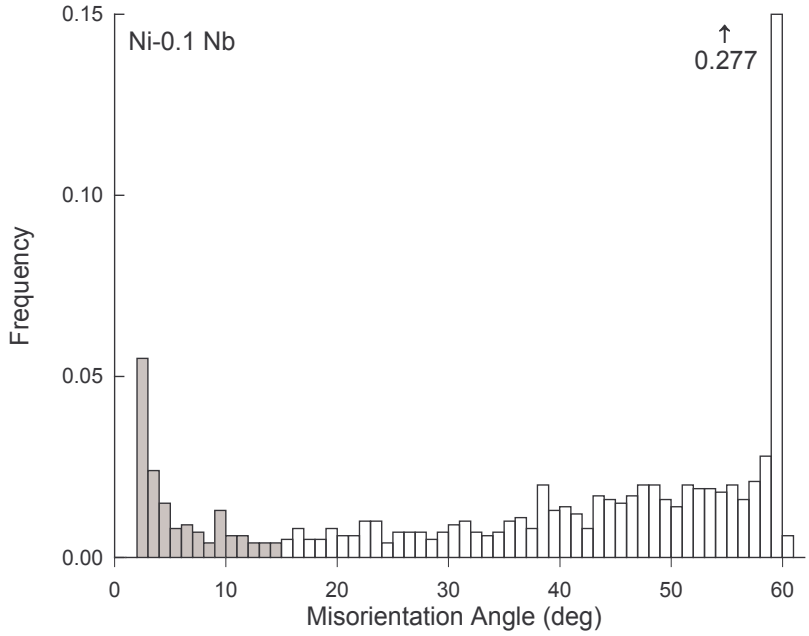
Ni-0.1 Nb
↑
0.277
Frequency
0.15
0.10
0.05
0.00
0
10
20
30
40
50
60
Misorientation Angle (deg)

(b)

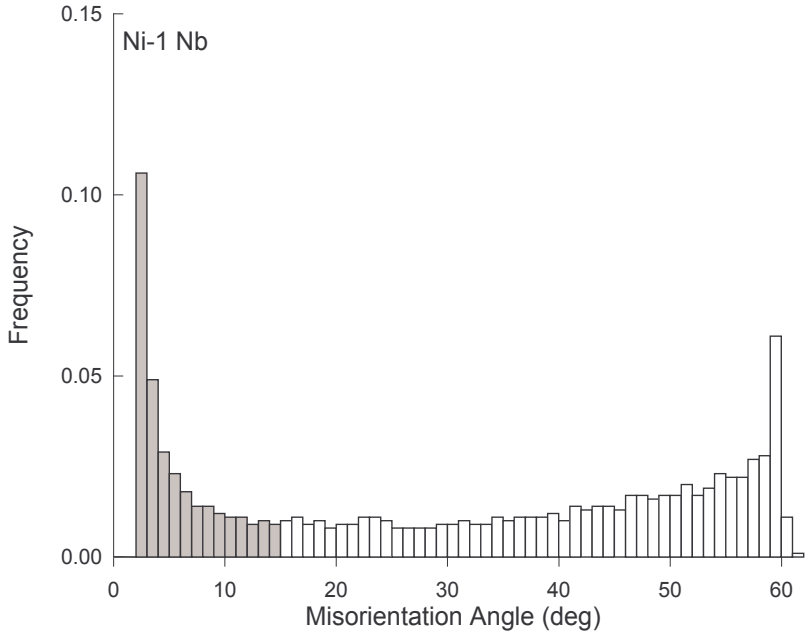

(c)

Figure 14. Misorientation angle distributions in pure nickel (a), Ni-0.1Nb (b), and Ni-1Nb (c) after torsion at 900 °C and 0.1 s^{-1} to a strain of 5. Subgrain boundaries are associated with grey bars.

It appears clearly from Figures 13 and 14 that the addition of niobium favours substructure development, as shown by the surface fractions of LABs which increase from about 0.02 for pure nickel, to 0.16 for Ni-0.1Nb, and 0.32 for Ni-1Nb. This may be due to the stabilization of dislocation walls by niobium solutes (*i.e.* decrease of dynamic recovery kinetics) and/or the decrease of grain boundary mobility, since substructure is usually swept out by moving grain boundaries.

By contrast, the twin boundary area fraction (here, by convention, boundaries with $59 < \theta < 61$ deg) is strongly reduced by niobium since it drops from 0.50 for pure nickel, to 0.28 for Ni-0.1Nb, and 0.07 for Ni-1Nb. The value of 0.50 for Ni is characteristic of a statically fully recrystallized low stacking fault energy metal (Gavard, 2001), which suggests that the microstructures in Figures 12a and 13a have undergone some post-dynamic evolution before quenching. The reduction of twinning by solutes has already been observed in other systems like Cu-Sn alloys (Bayle et al., 1999). It may be attributed to the decrease of grain boundary mobility since growth twinning during deformation is associated with grain boundary migration (Thomas, 2004).

Finally, the corresponding crystallographic textures are illustrated by {111} pole figures in Figure 15. In the case of pure nickel (Figure 15a), The pole figure does not exhibit any particular orientation, although it is not much significant due to the very large grain size. By contrast, a specific {111}<112> texture component is

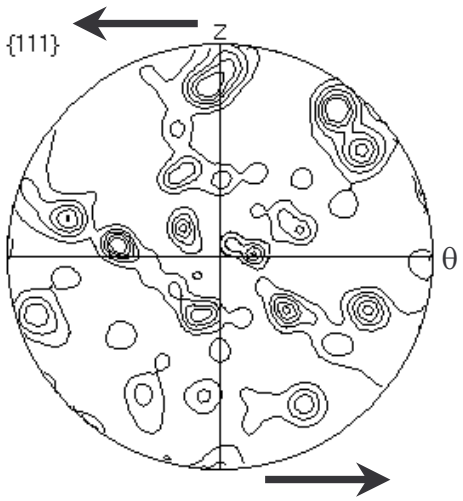

(a) min = 0.00 max = 6.91 levels = 1,2,3,4,5

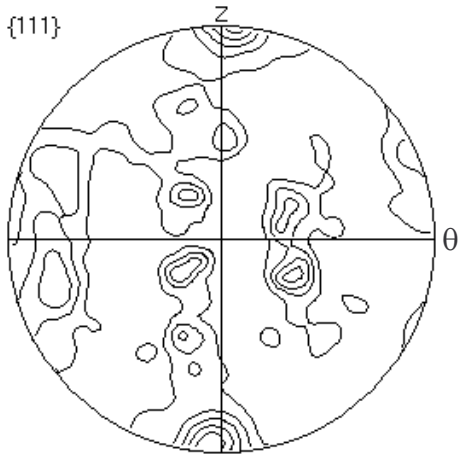

(b) min = 0.01 max = 5.94 levels = 1,2,3,4,5

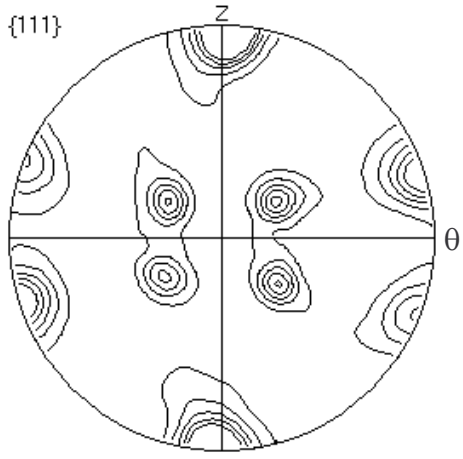

(c) min = 0.08 max = 10.21 levels = 1,2,3,4,5

Figure 15. {111} pole figures for pure nickel (a), Ni-0.1Nb (b), and Ni-1Nb (c) after torsion at 900 °C and 0.1 s^{-1} to a strain of 5. Arrows indicate the shear direction.

apparent for Ni-0.1Nb, that becomes very well pronounced for Ni-1Nb. (Here, {hkl} denotes the shear plane perpendicular to the z axis, and <uvw> the shear direction parallel to the θ axis). Such component has been referred to as A* (Montheillet et al., 1984), where the superscript star means that the shear direction <112> does not coincide with a classical slip direction for the fcc structure. More precisely, this component is made of two ideal orientations, *viz.* A_1* and A_2*, symmetric with respect to the shear plane. Each of the two is *self-symmetric* in the sense that it fulfills by itself the symmetry requirements of the torsion test (simple shear).

It should be noted that such texture component has not been previously observed in fcc metals submitted to large strain hot torsion testing: in low stacking fault energy metals, like the austenitic stainless steels, repeated twinning events randomize the grain orientations, such that texture is quite weak (Gavard, 1999), whereas in high stacking fault energy materials (aluminium alloys), the component $B/\overline{B}$, *i.e.* {112}<110> has been systematically observed (Montheillet et al., 2000).

Another point of interest is the co-existence in Ni-1Nb of the strong texture and a significant amount of twin boundaries (see Figures 13c and 14c). One can argue that the twinning rate is not sufficient in this case to randomize the grain orientations. It is also worth to remark that twinning on the {111} plane that coincides with the shear plane transforms the orientation A_1* into A_2* and vice-versa. This is consistent with the fact that grain orientations on both sides of a twin boundary are often both of the A* type, as illustrated in Figure 16. Therefore, the A_1*/A_2* set can be considered as partially stable under twinning, which may explain the above observations.

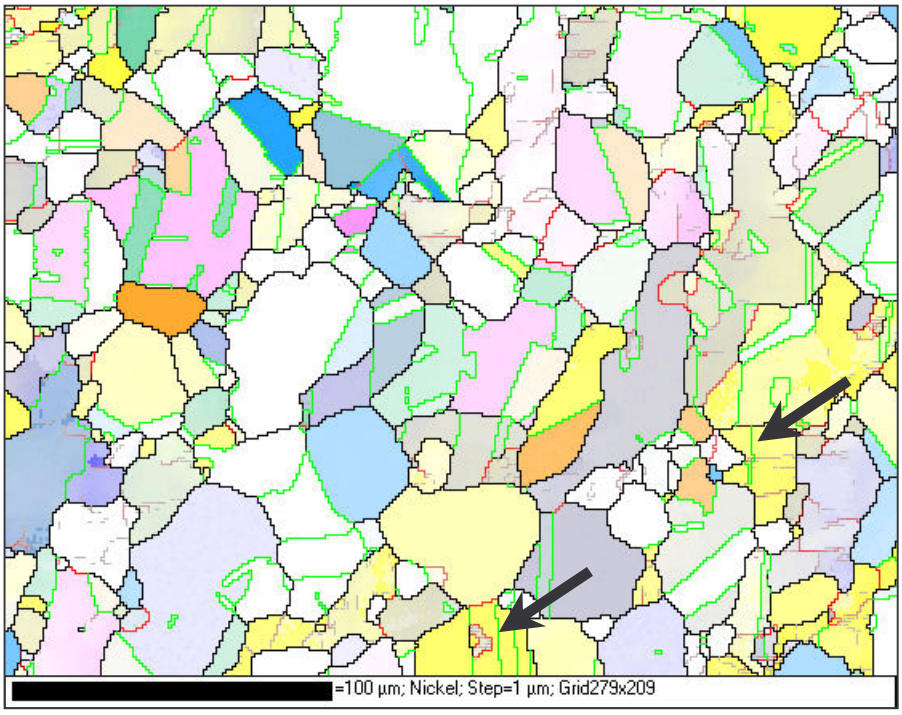

Figure 16. EBSD orientation map of Ni-0.1Nb after torsion at 900 °C and 0.1 s^{-1} to a strain of 5. Arrows show twin boundaries separating grains with orientation A* (yellow)

VI. CONCLUSIONS

Although it was quite limited in time and only a few number of specimens were used, this first investigation allows some interesting conclusions to be drawn:

(i) High purity nickel and two nickel base model alloys containing 0.1 and 1 wt%Nb, respectively, were prepared and transformed into torsion specimens in satisfactory conditions. In particular, there was no evidence of inhomogeneous niobium distributions in the initial as well as deformed microstructures.

(ii) Stress-strain curves suggest that hot deformation of the three materials is associated with discontinuous dynamic recrystallization. However, the kinetics of flow softening is decreased by niobium solutes.

(iii) The product mQ of the strain rate sensitivity and the apparent activation energy of deformation is remarkably independent of temperature, while m slightly increases (and therefore Q decreases) with growing temperature within the investigated range 800-1000 °C.

(iv) The strain rate sensitivity m is significantly reduced by the presence of niobium in solid solution, whereas Q is increased. These variations are more rapid between pure nickel and Ni-0.1 Nb than with further Nb addition, which means that a saturation effect occurs.

(v) Deformation microstructures associated with steady state flow stress ($\varepsilon = 5$) are considerably refined by niobium solutes. Furthermore, the addition of Nb favours substructure development while it reduces (growth) twinning during deformation.

(vi) To a first approximation, conclusions (iv) and (v) above can be summarized by saying that the addition of niobium in solid solution is tantamount to decrease the deformation temperature.

(vii) Finally, whereas no deformation texture is apparent in pure nickel, a well developed A_1^*/A_2^*, *i.e.* {111}<112> component forms in Ni-1Nb. The latter is partially stable with respect to twinning that still occurs in this alloy.

Starting from the above results, longer-term future work could be carried out with the aim of understanding and controlling the hot working of Ni base superalloys such as alloy 718. The following items could be dealt with:

- The investigation of hot deformation behaviour of a model Ni-Nb alloy containing only 100 ppm (or even less) niobium, to determine the solute concentration necessary to reach the above-mentioned "saturation effect" (see Figures 7, 9, and 10).

- On the other side, the investigation of Ni-Nb alloys containing large amounts of Nb (≈ 5 wt%), either in solid solution or partially in the form of

intermetallic precipitates Ni_3Nb, according the deformation temperature and initial heat treatment.

- The investigation of the same alloys with an addition of carbon, which is expected to influence Nb diffusion, and therefore modify the hot deformation mechanisms.

- Other Ni, Ni-Cr, or Ni-Cr-Fe base model alloys could be prepared and investigated, to understand the hot working behaviour of specific commercial superalloys.

- In parallel with the above experimental investigations, hot deformation models including continuous as well as discontinuous dynamic recrystallization, which have been developed in our laboratory, could be modified to explicitly include the effects of solutes and precipitates. This would allow the experimental data to be introduced into a theoretical frame, and to build a physically based model for the hot deformation of superalloys, able to predict the flow stress behaviour as well as the final microstructures.

REFERENCES

B. Bayle, Ph. Bocher, J.J. Jonas and F. Montheillet
Flow stress and recrystallization during the hot deformation of Cu-9%Sn alloys. *Mater. Sci. Technol.* **15**, 803-811 (1999).

L. Gavard
Recristallisation dynamique d'aciers inoxydables austénitiques de haute pureté. PhD Thesis, Ecole des Mines de Saint-Etienne/INPG (2001).

J. Le Coze, R. Tardy, A. Kobylanski and M. Biscondi
Preparation of high purity metals and metallurgical studies at the Ecole des Mines from 1970. Review. *Proc. 1st Int. Conf. on Ultra High Purity Base Metals (UHPM-94)*, Kitakyushu-City, Japan, p.371-389 (1995).

M.J. Luton and C.M. Sellars
Dynamic recrystallization in nickel and nickel-iron alloys during high temperature deformation. *Acta Metall.* **17**, 1033-1043 (1969).

F. Montheillet, M. Cohen and J.J. Jonas
Axial stresses and texture development during the torsion testing of Al, Cu and α-Fe. *Acta Metall.* **32**, 2077-2089 (1984).

F. Montheillet, S. Gourdet and C. Chovet
Dynamic recrystallization in aluminium alloys. *39th Conference of Metallurgists (COM'2000)*, *Light Metals 2000 Symposium,* Ottawa, Ontario, p.539-551 (2000).

J.-Ph. Thomas
PhD Thesis, Ecole des Mines de Saint-Etienne, to be published (2004).